A model for tip vortex roll-up in the near field region of three-dimensional foils and the prediction of cavitation onset

J.-A. Astolfi [a,*], D.H. Fruman [b], J.-Y. Billard [a]

[a] *Laboratoire d'Hydrodynamique de l'Ecole Navale, 29240 Brest Naval, France*
[b] *Groupe Phénomènes d'Interface, E.N.S.T.A, 91120 Palaiseau, France*

Abstract – A research program known as "Action Concertée Cavitation" initiated in France in 1991 was aimed at investigating Tip Vortex Cavitation (TVC) in various experimental facilities operating over a large range of Reynolds numbers. An original method to analyze the numerous data collected during the program was developed. From this method, a correlation model of the roll-up process close to the tip (near field region) of elliptical loading foils is proposed. It is based on the experimental evidence of a linear relationship, during the roll-up process, between a and $(\Gamma t)^{0.5}$, where a is the local vortex core radius, Γ the local vortex intensity and t the convection time. The core radius and the vortex intensity are modeled with power laws in such a way the linear relationship is satisfied. With the hypothesis of an axisymmetric vortex, the minimum of the pressure coefficient on the vortex path is computed. It agrees well with the experimental critical cavitation number obtained for lift coefficients ranging from 0.2 to 0.6 and for Reynolds numbers ranging from 4×10^5 to 6×10^6. Moreover, the model shows that the actual vortex diffusion appears to be faster than that predicted by laminar flow hypothesis. This can be explained by an apparent viscosity of about two orders of magnitude larger than the molecular viscosity during the roll-up process. Finally, as the model is based on a limited number of parameters to describe a complex phenomenon, it indicates also some important trends which should be examined by those seeking to mitigate the occurrence of cavitation on lifting surfaces as designers of pumps, propellers and other fluid machinery. © Elsevier, Paris

tip vortex cavitation / prediction

1. Introduction

Wing tip vortices are very strong coherent structures which have a great impact on aerodynamic and hydrodynamic applications. Many numerical and experimental works have been mainly concerned with the diffusion of the tip vortex in the far field region, beyond the position where the roll-up is achieved, see, for instance, Chigier and Corsiglia [1]; Baker et al. [2]; Zeman [3] and Devenport et al. [4]. More recent research has concentrated on the near field region, over a distance of a wing chord from the tip, because the first cavitation events occur in this region, initiating the development of Tip Vortex Cavitation (TVC) [5–10].

The main objective of the TVC studies is to predict cavitation inception for prototypes operating at Reynolds numbers larger than 10^7 by extrapolating the results obtained in reduced scale cavitation tunnels where Reynolds numbers are usually of less than 10^6. To do so, a cooperative research program known as 'Action Concertée Cavitation' (ACC) (see [11]) was initiated in France in 1991 [12]. Using the same experimental procedures in different experimental facilities operating over a large range of Reynolds number, the aim was to investigate the effect of foil planform [13], foil section [14], Reynolds number [15], upstream turbulence [16], foil unsteadiness [17], foil confinement [18,19] and oxygen and nuclei content [20,21]. Cavitation inhibition was also investigated by polymer solution ejection at the foil tip [22]. A considerable amount of data pertaining

---

* Correspondence and reprints; email: astolfi@ poseidon.ecole-navale.fr

to the inception cavitation number, the axial and tangential velocity profiles of the vortex in the near field region of a variety of foils with an elliptical loading is today available (see [11]). The aim of velocity measurements is to determine the minimum pressure on the vortex path to be compared to the critical cavitation number σ for which the cavitation appears (inception, $\sigma = \sigma_i$) or vanishes (desinence, $\sigma = \sigma_d$).

From several tangential velocity profile measurements, Fruman et al. [7], determined a, the local core radius, and Γ, the local vortex intensity at several locations along the vortex path. With the assumption of an axisymmetric vortex flow and the radial equilibrium equation, the local core vortex pressure coefficient was estimated along the vortex path, $C_P \sim (\Gamma/a)^2$. The position and the value of the minimum pressure coefficient $C_{P_{\min}}$ were then determined and compared to the critical cavitation number. In spite of the simplifying assumption of an axisymmetric vortex flow and although the actual pressure for cavitation depends on the spectrum of bubbles present in the inception region [20], it has been found that $-C_{P_{\min}}$ was in good agreement with the desinent cavitation number particularly if a susceptibility pressure is used in the definition of the critical cavitation number—instead of the vapor pressure—to take into account the water quality (see [12]). However, as it can be seen, $C_{P_{\min}}$ is strongly dependent on a reliable estimation of a and Γ.

In order to extrapolate the results from reduced scale cavitation tunnel to prototypes, great efforts have been made to scale the experimental data (as a, Γ) with the flow conditions as Reynolds number, Re, and the lift coefficient C_l, for instance. On this point, several authors such as Billet and Holl [5] and Fruman et al. [7] assume that the vortex core a is related to the boundary layer thickness δ. This hypothesis leads to a dependence on the Reynolds number, $a \sim \delta \sim cRe^{-n}$, with $n = 0.2$ for a fully turbulent boundary layer (c is the root chord) and $n = 0.4$ for the original McCormick [23] hypothesis which appears reasonable for a transitional boundary layer as suggested by Maines and Arndt [10]. Concerning Γ, Fruman et al. [7] assume that it is related to Γ_0, the root circulation which is $\Gamma_0 = 0.5U_\infty C_l c$, for hydrofoils with an elliptical loading, where U_∞ is the free stream velocity. Both scaling hypotheses on a and Γ together with $C_P \sim (\Gamma/a)^2$, lead to the relation, $C_{P_{\min}} = -K_{C_{P_{\min}}} C_l^2 Re^{2n}$, where n is a positive exponent depending on the boundary layer development on the foil surface and $K_{C_{P_{\min}}}$ a positive constant probably governed by the local geometry of the foil tip. Concerning critical cavitation number, several authors have predicted that it should follow the relation $\sigma_d \sim K_{\sigma_d} C_l^2 Re^m$ where K_{σ_d} is a positive constant depending on the hydrofoil section. Platzer and Souders [24] proposed $m = 0.36$ in agreement with Mc Cormick's result. More recently, Billet and Holl [5], Fruman et al. [7] and Maines and Arndt [10] suggested that a better correlation of inception data is achieved with $C_l^2 Re^{0.4}$ for hydrofoils with an elliptical loading. From these numerous studies, it appears that reliable methods to study TVC data are still needed. For instance, methods to estimate the minimum pressure coefficient on tip vortices make an interesting way to predict cavitation inception (see [25,26] and recently, [27]). Moreover, these methods could suggest trends to delay cavitation inception.

In this paper, a method is developed to analyze the numerous data collected during the ACC program. From the analysis of the experimental values of a and Γ, a correlation model describing the tip vortex roll-up process (a and Γ evolution) in the region extending from the foil tip up to a maximum chord downstream is proposed. Based on the scaling relationships hypothesized above ($a \sim \delta$, $\Gamma \sim \Gamma_0$ and $C_P \sim (\Gamma/a)^2$) the value and the location of the minimum pressure coefficient on the vortex path could be predicted. Moreover, it provides a very concise presentation of numerous experimental tests and should be very useful for further TVC data analysis.

The paper is organized as follows. It begins with the presentation of previously published results concerning tip vortex characteristics (Section 2). Then, the basic formulation of the model is presented (Section 3) and followed (Section 4) by the description of the data fitting procedure for a and Γ. The results of the model are presented and discussed in Section 5.

2. Summary of previous results

2.1. Experimental procedure

Since the main objective of the paper is to propose a model based on a large amount of measurements of the axial and tangential tip vortex velocity profiles, as well as foils characteristics, such as lift coefficient and critical cavitation numbers, it seems appropriate to provide some information on the experimental procedures—instrumentation, facilities and methods—used to obtain the data and their uncertainty bounds. A large part of the data used in the present work, were obtained in our laboratory and the results were compared to independent tests conducted in the other laboratories. For more details in the experimental procedures, readers should refer to the paper by Fruman et al. [7].

The experiments were conducted in different size cavitation tunnels, with test section dimensions ranging from about 0.1 m to 1 m. In all of the tunnels but one, the hydrofoils were mounted horizontally on one of the vertical walls of the test section and axial and vertical (or tangential) velocities were measured along an axis parallel to the span of the foil for up to twelve stations located between the foil tip and a chord downstream, (see *figure 1* for coordinate definition).

A two component DANTEC^{TM} LDV system operating in the back scattering mode was used to measure the velocities. For the optical configurations used in our facility, the measuring volume was 0.5 mm long and 0.04 mm wide. The velocity profiles are defined with spatial steps which were as small as 40 μm in the core region where the variation of the velocity is very large. In order to quantify tip vortex characteristics at each stage of the roll-up process, a local vortex intensity, $\Gamma(x)$, and a local viscous core radius, $a(x)$ can be inferred from the information contained in the tangential velocity profiles using the following procedure:

(i) The angular momentum, product of the tangential velocity by the distance to the vortex axis, is plotted as a function of the distance to the vortex axis. In general, outboard of the foil, a nearly constant value is achieved well outside the viscous core. This value is then selected as $\Gamma(x)(2\pi)^{-1}$.

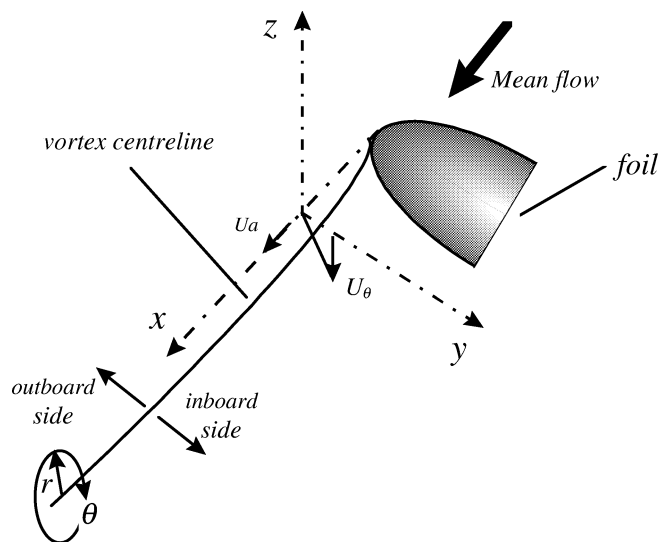(ii) The vortex core radius $a(x)$ is defined by the position of the maximum of the tangential velocity.

Figure 1. Schematic of the test arrangement showing the coordinate system. The origin is at the foil tip. U_a and U_θ are the axial and tangential (vertical) velocity components.

(iii) Using the value of $\Gamma(x), a(x)$, and $U_{\theta_{max}}$ it is easy to verify if the experimental velocity profile can be approached by a Lamb type vortex,

$$U_\theta(x,r) = \frac{\Gamma(x)}{2\pi r}\left(1 - e^{-1.255r^2/a^2}\right) \tag{1}$$
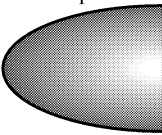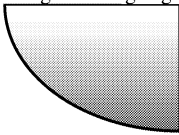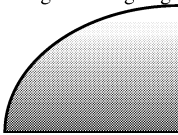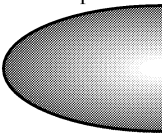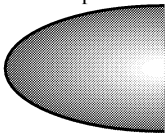
by verifying that

$$\frac{0.714\Gamma(x)}{2\pi a(x)U_{\theta_{max}}} \approx 1. \tag{2}$$

It has been shown that in most cases, and especially in the near-field region, the fit of the experimental velocity profile by a Lamb profile was satisfactory [7].

(iv) With the hypothesis of an axisymmetric vortex, an estimate of the pressure coefficient can then be obtained using the simplified radial equilibrium equation (in which it has been assumed that the radial velocity is negligible) either by numerical integration of the experimental tangential velocity profile or by using analytical integration of a Lamb profile, $C_P = -0.044[\Gamma/(U_\infty a)]^2$.

The geometric characteristics of the foils, the Reynolds numbers, Re, the incidence angles, the lift coefficients, C_l, and the desinent cavitation numbers, σ_d, are summarized in *table I*. Data for foils with an elliptical loading but with different cross sections and planforms will be used in this work [7,14,22]. For a NACA 16-020 cross section (maximum thickness located at mid-chord), one foil has an elliptical planform (E) while the two others were shaped like a quarter of ellipses; one with a straight leading edge (SLE) and the other with a straight trailing edge (STE). They are respectively referred to as 16020E, 16020SLE and 16020STE. Because of the peculiar lift characteristics of the 16020E foil, experiments have been also conducted by tripping the boundary layer laminar-turbulent transition [15]. For a NACA 0020 cross section (maximum thickness located at 30% of the section chord length), only the elliptical shape was studied and will be referred to as 0020E. Moreover, the results obtained when ejecting a polymer solution from the tip of the 16020E foil will be referred to as 16020E POLY [22].

Table I. Experimental conditions and values of σ_d and K_{σ_d}.

section	16-020				16-020		16-020		0020			16-020
	elliptic				straight leading edge		straight trailing edge		elliptic			elliptic
planform												
reference	16020E				16020SLE		16020STE		0020E			16020E POLY
chord [m]	0.08				0.08		0.08		0.08			0.08
span [m]	0.12				0.12		0.12		0.12			0.12
R_e x10^{-6}	0.4 tripped	0.56 tripped	1.08	1.2	1.08	1.2	1.08	1.2	0.56	0.92	0.92	1 polymer ejection
incidence	10°	6°	10°	6°	10°	6°	10°	6°	10°	10°	6°	10°
C_l	0.44	0.25	0.35	0.20	0.37	0.27	0.36	0.21	0.61	0.61	0.37	0.35
σ_d	1.62	0.59	1.60	0.83	1.60	0.48	1.6	0.48	5.5 ↑	2.9	0.95	1.4
K_{σ_d}	0.049				0.041		0.049		0.037			0.039

↑ in that case a small cavity on the foil surface at the foil tip occurred together with tip vortex cavitation·

2.2. Evolution of the tip vortex core radius and intensity

It can be shown (see *figures 2(a)–2(e)*) that for a variety of foils, incidence angles and/or Reynolds numbers the evolution of the core radius, a, scales with δ, the turbulent boundary layer thickness of a flat plate of length equal to the maximum chord, c, with a constant of proportionality depending on the foil shape. This allows us to define a nondimensional core radius,

$$a^* = \frac{a}{\delta} = \frac{a}{0.37cRe^{-0.2}}. \tag{3}$$

$Re = U_\infty c/\nu$ is the Reynolds number, U_∞ is the upstream flow velocity and ν is the fluid kinematic viscosity. In the same way, the local vortex intensity Γ, scaled with the mid-span circulation Γ_0 (computed from the measured lift coefficient, C_l) allows us to define a nondimensional vortex intensity,

$$\Gamma^* = \frac{\Gamma}{\Gamma_0} = \frac{\Gamma}{0.5C_l U_\infty c}. \tag{4}$$

From repeated applications of the procedure to measure the vortex core radius and the local vortex intensity, the standard deviations for a^* and Γ^* were estimated at 13 and 10%, respectively.

2.3. Critical desinent cavitation number

The desinent cavitation number, σ_d, is defined as follows,

$$\sigma_d = \frac{p_\infty - p_v}{0.5\rho U_\infty^2} \tag{5}$$

where p_∞ is the reference pressure at which tip vortex cavitation disappears, p_v is the vapor pressure at ambient temperature and ρ is the fluid specific mass. As an example, *figure 3* displays σ_d divided by $Re^{0.4}$ as a function of the square of the lift coefficient. Despite some scatter, the data can be quite well fitted by a straight line of the form

$$\frac{\sigma_d}{Re^{0.4}} \approx K_{\sigma_d} C_l^2. \tag{6}$$

The values of K_{σ_d} are summarized in *table I*.

2.4. Axial velocities

The distribution of core vortex axial velocities scaled with the free-stream velocity U_∞ are shown in *figure 4* for the experimental conditions of *table I*. Either a jet or a wake behavior is observed depending on the foil section and planform. The magnitude of the excess (or defect) depends on the incidence of the foil. When moving downstream, the data approaches the free-stream velocity. For instance the 0020E, 16020E and 16020SLE foils display, in general, a jet behavior with a velocity excess of up to 30% whereas the 16020STE foil displays a very marked wake behavior with a maximum velocity defect of 75%. This can be interpreted as a boundary layer effect on this foil which strongly decelerates the incoming fluid passing on the foil. Polymer solution ejection at the foil tip of the 16020E foil leads to a pronounced wake behavior [22].
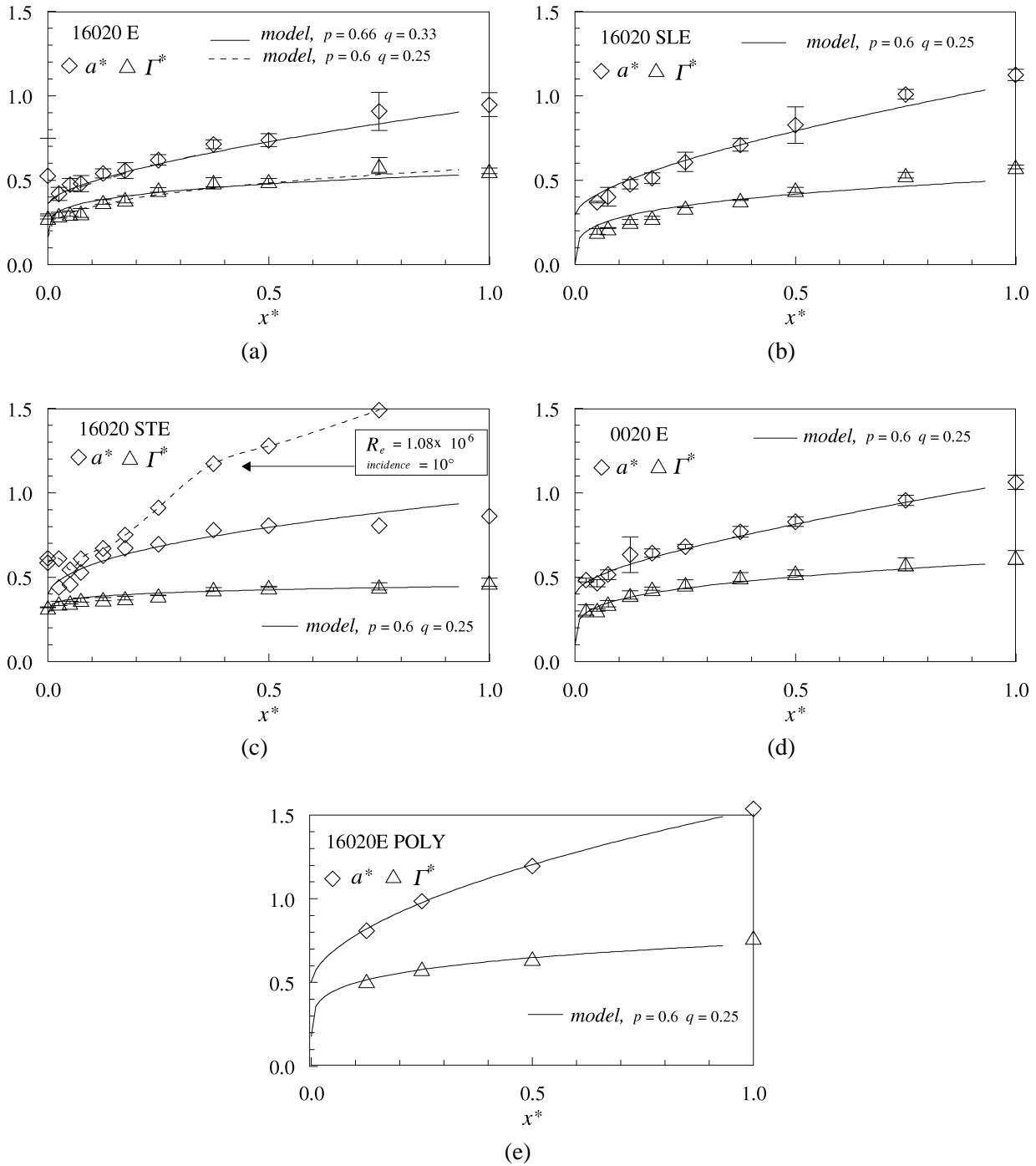
Figure 2. Nondimensional tip vortex radius and intensity as a function of the nondimensional distance from the foil tip. Symbols and vertical bars are the averaged experimental values and the standard deviations obtained from experimental conditions given in *table I*. Continuous or dashed lines correspond to power law models. (a) 16020E, (b) 16020SLE, (c)16020STE (d) 0020E, (e) 16020E POLY.
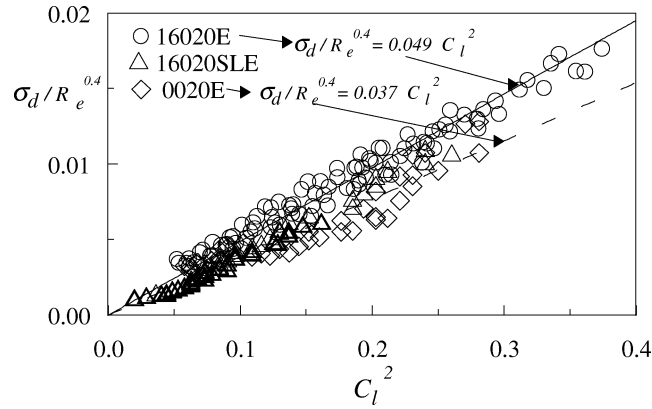
Figure 3. Desinent cavitation number divided by the Reynolds number to the power 0.4 as a function of the square of the lift coefficient for three foils. The continuous and dashed lines are linear fits through the 16020E and 0020E foil data, respectively. Experimental conditions are given in *table I*.
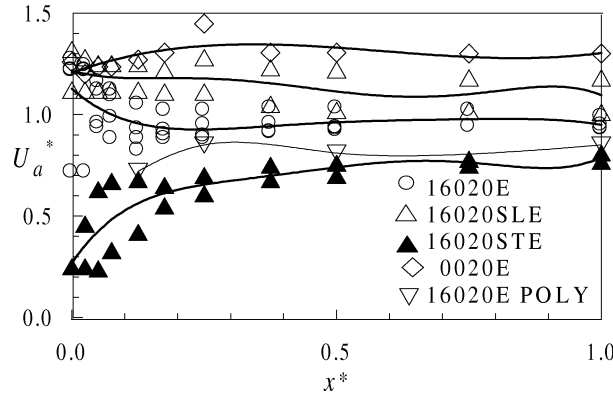

Figure 4. Nondimensional axial velocity in the vortex core as a function of the nondimensional distance from the foil tip. Experimental conditions are given in *table I*.

3. Model formulation

3.1. a^* and Γ^* formulation

It will be assumed that a^* and Γ^* can be well represented by a power law of the nondimensional time needed for a fluid particle to travel the distance from the foil tip (transit time), $t^* = tU_\infty/c$:

$$a^* = \alpha_0\left(1 + \alpha t^{*p}\right), \tag{7a}$$

$$\Gamma^* = \gamma_0\left(1 + \gamma t^{*q}\right). \tag{7b}$$

The exponents p and q are positive numbers and indicate respectively the temporal evolution of the vortex core diffusion and the roll-up process. For instance, in the case of a laminar flow where diffusion is controlled by molecular viscosity, if the roll-up process is completed, q should be equal to zero, and p should be equal to 0.5. The parameters α_0 and γ_0 are the initial nondimensional core radius and intensity for $t^* = 0$ (or $x^* = 0$), α and γ express the radius and intensity growth rate at $t^* = 1$. The parameters need to be empirically determined for each tested foil.

3.2. Transit time

In Eq. (7) t^* is defined as

$$t^* = \int_0^{x^*} \frac{dx^*}{U_a^*(r=0, x^*)} \tag{8}$$

where $U_a^*(r=0, x^*)$ is the axial velocity in the vortex core scaled with U_∞ and r is the radial distance to the vortex axis. Based on experimental evidence, it is assumed to be of the form

$$U_a^* = \frac{U_a}{U_\infty} = \left(1 + k_1 e^{-k_2 x^*}\right) \tag{9}$$

where k_1 positive (respectively negative) indicates a jet (respectively a wake) behavior. The value of k_1 quantifies the excess or the defect of the velocity at the foil tip and is assumed in the present model to be independent of the Reynolds number and of the lift coefficient. The constant k_2 is positive and quantifies the free-stream velocity recovery downstream the foil tip. Integrating Eq. (8), we have

$$t^* = -\frac{1}{k_2} \left\{ \log\left|1 - \frac{1}{1 + k_1 e^{-k_2 x^*}}\right| - \log\left|1 - \frac{1}{1 + k_1}\right| \right\} \tag{10}$$

which allows a direct computation of t^* as a function of x^*.

3.3. Vortex core pressure estimate

The tangential velocity profiles can be fitted quite well by a Lamb velocity model in the very near field region. As discussed by Fruman et al. [7], the pressure coefficient can be rather well estimated by integrating the simplified radial equilibrium equation

$$C_P = \frac{p_{r=0} - p_\infty}{0.5 \rho U_\infty^2} = -0.044 \left[\frac{\Gamma}{U_\infty a}\right]^2 \tag{11}$$

where $p_{r=0}$ is the pressure in the vortex axis and p_∞ the reference pressure far away from the vortex core. According to Eqs (3), (4) and (7) we have

$$C_P(t^*) = -0.0803 \frac{\gamma_0^2}{\alpha_0^2} f(\alpha, \gamma, t^*) C_l^2 Re^{0.4} = K_{C_P}(t^*) C_l^2 Re^{0.4} \tag{12}$$

with

$$f(\alpha, \gamma, t^*) = \left(\frac{1 + \gamma t^{*p}}{1 + \alpha t^{*q}}\right)^2 \tag{13}$$

and, as $f(\alpha, \gamma, t^*)$ is positive, we have

$$C_{P_{\min}} \propto -f_{\max}. \tag{14}$$

Equation (12) allows the computation of the pressure coefficient in the vortex core provided (γ_0/α_0) as well as α and γ are known. It is then possible to compute $C_{P_{\min}}$, to determine the time for which it occurs, $t_{\min}^*$, and using the inverse of Eq. (10) to determine the distance from the foil tip, $x_{\min}^*$.

4. Fitting procedure

4.1. Physical discussion, vortex growth parameter

Zeman [3], using scaling arguments showed that, for the far region where roll-up is completed, a scales with $(\Gamma_0 t)^{0.5}$ where Γ_0 is the wing circulation given by the wing lift. He showed that the vortex core growth parameter, given by

$$b_1 = \frac{\Delta a}{\Delta(\Gamma_0 t)^{0.5}} \tag{15}$$

is a power law function of the Reynolds number, defined as, $Re_\Gamma = \Gamma_0/\nu$, with an index close to -0.5 implying $a \sim (\nu t)^{0.5}$, which suggests viscous rather than turbulent diffusion of the vortex. It is interesting to extend the approach of Zeman [3] into the near region by plotting a^* as a function of $(\Gamma^* t^*)^{0.5}$ for each tested configuration. This is done in *figures 5(a)–5(e)*. As opposed to the Zeman situation, where Γ_0 is constant, here Γ^* progressively increases from the foil tip to take into account the roll-up process.

In *figures 5(a)–5(e)* a very good linear dependency between a^* and $(\Gamma^* t^*)^{0.5}$ is achieved:

$$a^* \approx \alpha_0 + b_1^* \left(\Gamma^* t^*\right)^{0.5}. \tag{16}$$

Only in the case of the 16020STE foil for one case (*figure 5(c)*), there is a departure for $(\Gamma^* t^*)^{0.5} > 0.5$. The vortex growth parameter is now given by

$$b_1 = \frac{\Delta a}{\Delta(\Gamma t)^{0.5}} = 0.37 b_1^* \left(\frac{\Gamma_0}{\nu}\right)^{-0.5} Re^{0.3} \tag{17}$$

with

$$b_1^* = \frac{\Delta a^*}{\Delta(\Gamma^* t^*)^{0.5}}. \tag{18}$$

For an elliptical loaded foil, we have

$$b_1 \propto \left(\frac{C_l}{2}\right)^{-0.5} Re^{-0.2}. \tag{19}$$

Equation (17) shows, in addition to $Re_\Gamma^{-0.5}$, a dependency on Re^m with $m = 0.3$, which can be interpreted as the influence of the foil Reynolds number through the boundary layer effects.

As Ferreira De Sousa and Falcao De Campos [27] rightly pointed out, the quantitative prediction of the minimum pressure in the vortex core is critically dependent on the estimate of the viscous core radius at the foil tip, α_0 (see Eq. (12)). As an interesting result of the linear evolution, *figures 5(a)–5(e)* show that it is possible to determine the initial radius by extrapolating the linear fits to the origin (see Eq. (16)). Because the estimation is based on the whole data, at the tip and away from it, it is better than that obtained from only one measurement at the foil tip. For the 16020E foil a value of 0.36 is obtained from the whole data concerning this wing. This compares favorably with the value of 0.32 estimated by Ferreira De Sousa and Falcao De Campos [27].
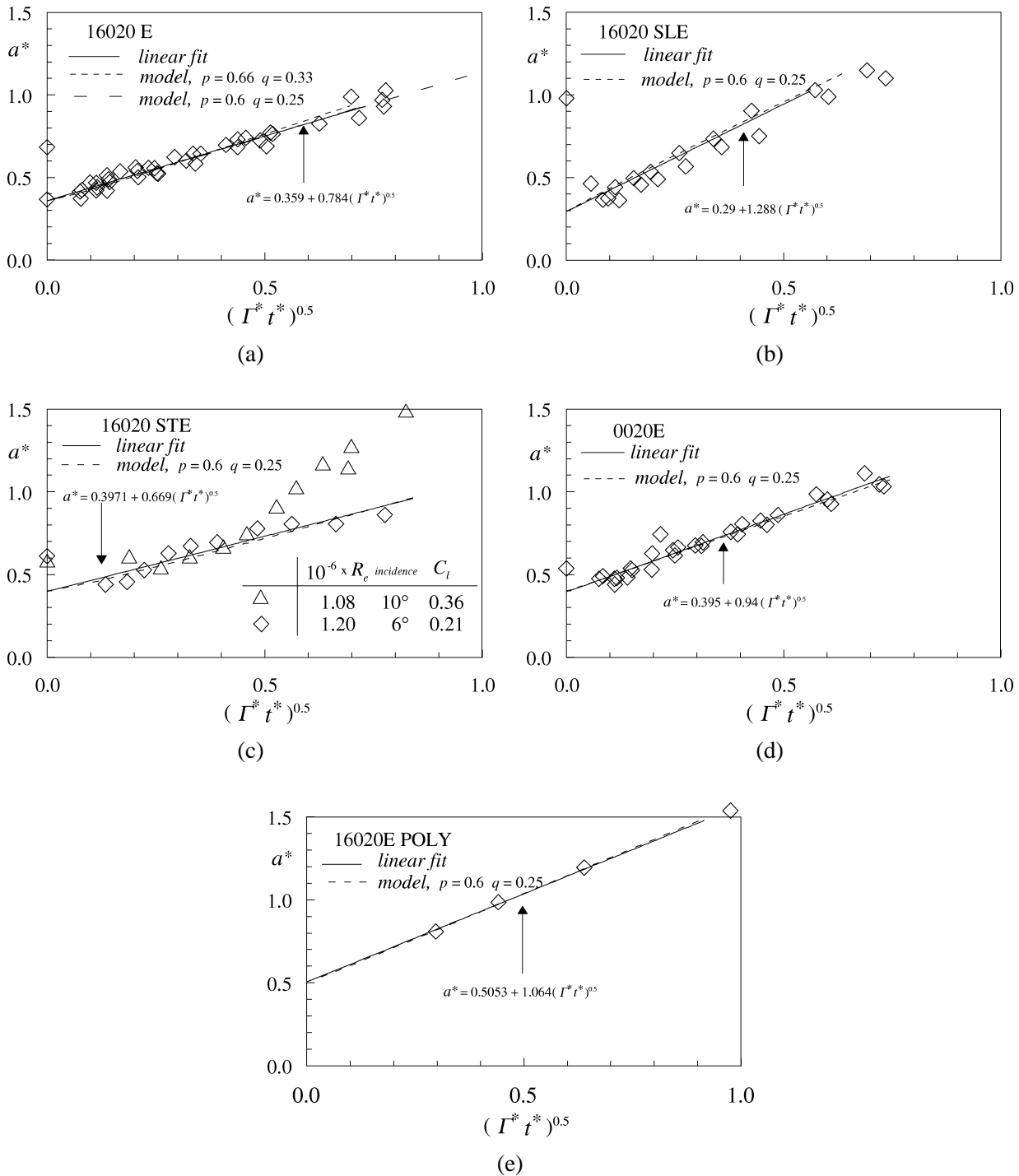
Figure 5. Nondimensional tip vortex radius as a function of $(\Gamma^* t^*)^{0.5}$ for foils: (a) 16020E, (b) 16020SLE, (c) 16020STE, (d) 0020E, (e) 16020E POLY. Experimental conditions are given in *table I*.

4.2. *Exponents p and q*

We look for the values of exponents p and q in Eq. (7) such that $a^* \propto (\Gamma^* t^*)^{0.5}$. To do that let us write

$$a^* = \alpha_0 + b_1^* (\Gamma^* t^*)^{0.5} \tag{20}$$

which, after substituting Eq. (7) becomes

$$\alpha_0 (1 + \alpha t^{*p}) = \alpha_0 + b_1^* (\gamma_0 (1 + \gamma t^{*q}) t^*)^{0.5}. \tag{21}$$

By taking the square of Eq. (21), we have

$$t^{*2p} = \frac{\kappa}{\gamma} t^* + \kappa t^{*q+1} \tag{22}$$

with

$$\kappa = \frac{b_1^* \gamma_0 \gamma}{\alpha_0^2 \alpha^2}. \tag{23}$$

We look for the values of κ, γ, p and q for which Eq. (22) can be satisfied. This equation has no exact solution excepted for $\gamma \gg 1$, for which we should have

$$\begin{cases} 2p = q + 1 \\ \kappa = 1. \end{cases} \tag{24}$$

With $\gamma \gg 1$, Eq. (23) shows that $\gamma_0 \ll 1$ meaning that the roll-up process is initiated almost precisely at the foil tip. In the general case of the roll-up process initiated not strictly at the foil tip but along a part of the leading edge, γ_0 should have a finite value at the foil tip and γ should not be necessarily large. Thus, the parameters of Eq. (22) cannot be determined rigorously and a trial and error procedure, described below, is needed:

(a) We select one of the plots given in *figures 5(a)–5(e)*, say *figure 5(a)* for the 16020E foil, and determine, by extrapolation to the origin, the value of α_0.

(b) With this value of α_0 and the data from *figure 2(a)* for a^* and *figure 4* to compute t^*, we determine the coefficients of Eq. (7a) giving the best fit in the sense of a least square procedure,

$$a^* = 0.359 (1 + 1.76 t^{*0.66}). \tag{25}$$

(c) Because of Eq. (24), an initial value of $q = 2p - 1 = 1/3$ is selected. Using the data of *figure 2(a)* for Γ^* and *figure 4* to compute t^*, the coefficients of Eq. (7b) giving the best fit in the sense of a less square procedure are then determined,

$$\Gamma^* = 0.16 (1 + 2.6 t^{*0.33}). \tag{26}$$

(d) The coefficients and powers of expressions (25) and (26) are used to plot a^* as a function of $(\Gamma^* t^*)^{0.5}$ into *figure 5(a)* (dashed line), to be compared to the linear fit of the experimental data (continuous line). As shown, the agreement between the model and the experimental fit is rather good. Nevertheless, *figure 6* (dashed line) shows as a function of $(\Gamma^* t^*)^{0.5}$ the relative difference of a^* obtained using the model and the linear fit. In the very near region, the model underestimates a^* by up to 5% and it overestimates it by up to 10% for $(\Gamma^* t^*)^{0.5}$ larger than 0.35.
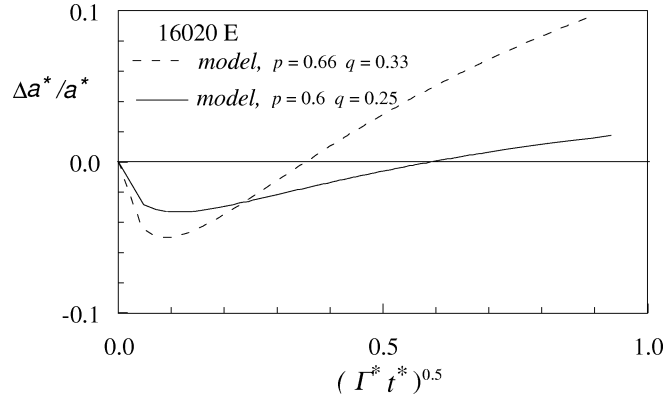
Figure 6. Relative difference of a^* between the linear fit and the model for the 16020E foil.

(e) This adjustment can be improved by adjusting the powers. After a trial and error procedure, we obtain

$$\begin{cases} a^* = 0.36\left(1 + 1.61t^{*0.6}\right) \\ \Gamma^* = 0.18\left(1 + 2.0t^{*0.25}\right). \end{cases} \tag{27}$$

This is shown graphically in *figure 2(a)* (replacing t^* by x^*), in *figure 5(a)* and *figure 6* (continuous line). This last one shows clearly that fitting has been improved with a relative difference of less than $\pm 4\%$.

(f) These powers are considered to be well representative of the tested conditions and used to fit the data for all of the other hydrofoils as shown in *figures 2(b)–2(e)* and *figures 5(b)–5(e)*.

The exponent $p = 0.6$ for the core radius evolution in Eq. (27) implies a more rapid diffusion than in the laminar case, for which

$$a = (5.02\nu t)^{0.5}. \tag{28}$$

Here in dimensional form, using (Eq. 7) with $p = 0.6$, we have

$$a - a_0 = \left(5.02\nu_T t^*\right)^{0.5} \tag{29}$$

with

$$\nu_T = 0.027\alpha^2\alpha_0^2 Re^{0.6}t^{*0.2}\nu. \tag{30}$$

ν_T can be considered as an apparent viscosity indicating that the actual tip vortex diffusion, during the roll-up process, can be larger than the one based on laminar flow assumptions. A mean value of ν_T, computed over a time T^* which could be considered as a characteristic time of the roll-up process, is:

$$\bar{\nu}_T = \frac{1}{T^*}\int_0^{T^*} \nu_T \, dt^* = 0.0225\alpha^2\alpha_0^2 Re^{0.6}T^{*0.2}\nu. \tag{31}$$

Setting that, T^*, is the time for which the roll-up process is completed, $\Gamma^* = 1$ in (Eq. 7b), we have

$$T^* = \left(\frac{1 - \gamma_0}{\gamma\gamma_0}\right)^{1/q} \tag{32}$$

Table II. Values of ξ and η as a function of γ.

γ	1	2	3	4	5
ξ	1.593	2.96	4.72	7.01	9.82
η	0.349	0.438	0.489	0.547	0.585

and, with $q = 0.25$, the apparent viscosity can be now related to the model constants as

$$\frac{\bar{v}_T}{v} = 0.0225\alpha^2\alpha_0^2\left(\frac{1-\gamma_0}{\gamma\gamma_0}\right)^{0.8} Re^{0.6}. \tag{33}$$

It may be noted that $\bar{v}_T$ is larger for full-scale situations because of the dependence on the Reynolds number to the power 0.6.

4.3. Minimum pressure coefficient

Eq. (14) indicates that $C_{P_{\min}} \sim -f_{\max}$. With $p = 0.6$ and $q = 0.25$, *figure 7* shows that, in logarithmic coordinates, the values of $f_{\max}$ display a near linear behavior as a function of α for each value of γ. $f_{\max}$ can be fitted then by

$$f_{\max} = \xi\alpha^{-\eta} \tag{34}$$

where ξ and η are coefficients depending on γ (*table II*), which in turn can be fitted by

$$\begin{aligned}\xi &= 0.774 + 0.5864\gamma + 0.244\gamma^2, \\ \eta &= 0.351\gamma^{0.321}.\end{aligned} \tag{35}$$

This gives when combining with Eq. (12),

$$C_{P_{\min}} = -0.0803\frac{\gamma_0^2}{\alpha_0^2}\xi\alpha^{-\eta}C_l^2 Re^{0.4} = K_{C_{P_{\min}}}C_l^2 Re^{0.4} \tag{36}$$

which allows one to rapidly compute $C_{P_{\min}}$ and shows the strong dependency on the initial conditions (α_0, γ_0).
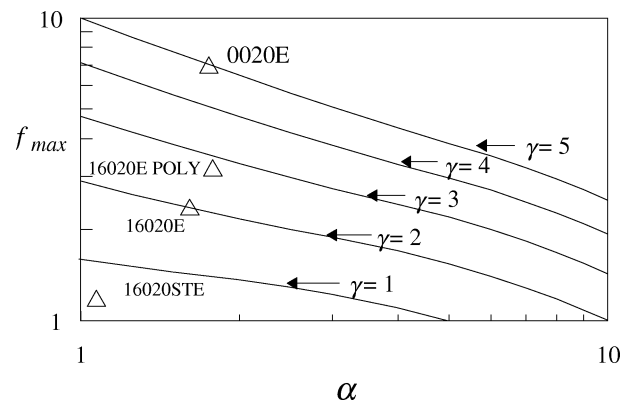

Figure 7. Maximum of $f(\alpha, \gamma, t^*)$ as a function of α for various values of γ. Symbols are the data for the tested foils.

Moreover, studying the function $f(\alpha, \gamma, t^*)$ in Eq. (13) with $p = 0.6$ and $q = 0.25$ together with Eq. (34), it can be shown that $f_{\max}$ (or $C_{P_{\min}}$) occurs when

$$t^*_{\min} = \left(5.76 \xi \alpha^{-\eta} \frac{\alpha^2}{\gamma^2} \right)^{-1/0.7}. \tag{37}$$

Using Eq. (10), we then have

$$x^*_{\min} = -\frac{1}{k_2} \log \left\{ \frac{1}{k_1} \left(\frac{1}{1 \pm K} - 1 \right) \right\} \tag{38}$$

with

$$K = \exp\left(\log \left| \frac{k_1}{1 + k_1} \right| - k_2 t^*_{\min} \right) \tag{39}$$

relating directly the position of the minimum pressure to the model constants. The positive (respectively negative) sign in Eq. (38) is used when simulating a wake effect, $k_1 < 0$, (respectively a jet effect, $k_1 > 0$) in the axial velocity profile. It can be shown that increasing α or decreasing γ causes the minimum pressure coefficient to move closer to the foil tip.

5. Results and discussion

Table III summarizes the values of all the parameters for the four foils and the polymer solution ejection together with their mean values and standard deviation. The core radius at initiation ranges from 30 to 50% of the boundary layer thickness with the largest value obtained with polymer ejection. The initial vortex intensity ranges from 10 to 30% of the root circulation. It is nearly zero for the 16020SLE foil because roll-up is initiated at the foil tip (Eq. (23) with κ very close to one and γ very large). For the 16020STE, it is the largest ($\gamma_0 = 0.28$), and 1.55 times larger than that of the intermediate 16020E foil, ($\gamma_0 = 0.18$). It can be speculated that the reason for such an increase in the initial vortex intensity is directly associated to the length of the leading edge over which the roll-up occurs. If it can be assumed that the roll-up is restricted to a small percentage of the span, say about 20% [28], the leading edge length over which the roll-up occurs for the STE foil should be 1.53 times larger than that of the E foil, very closed to 1.55, the ratio of the values of γ_0.

Whereas the initial conditions are close, the intensity growth rate, γ, is much larger for the 0020E foil ($\gamma = 5$) than for the 16020E foil ($\gamma = 2$). The consequence is a value of $K_{C_{P_{\min}}}$ larger by a factor of 1.34 times larger for the 0020 foil. This indicates that moving the maximum foil thickness towards the leading edge promotes the roll-up process and should be beneficial for delaying cavitation. It can be noticed that the ratio of 1.34 between the values of $K_{C_{P_{\min}}}$ is close to 1.4 ($= 0.7/0.5$) the ratio of the chord fractions beyond the maximum thickness.

As shown, except for the STE foil, the mean characteristic time for which the roll-up process is completed is of about 13 times the typical convection time c/U_∞.

5.1. Vortex core pressure coefficient and critical cavitation number

Figures 8(a)–8(d) show the evolution of $K_{C_{P_{\min}}}$ along the vortex path modeled using Eq. (12) and the constants of *table III*. It is compared with the average of the experimental values—together with standard deviation—obtained either by analytical integration of a Lamb profile or by numerical integration of the experimental tangential velocity. It must be pointed out that both values are (at least indirectly) inferred from
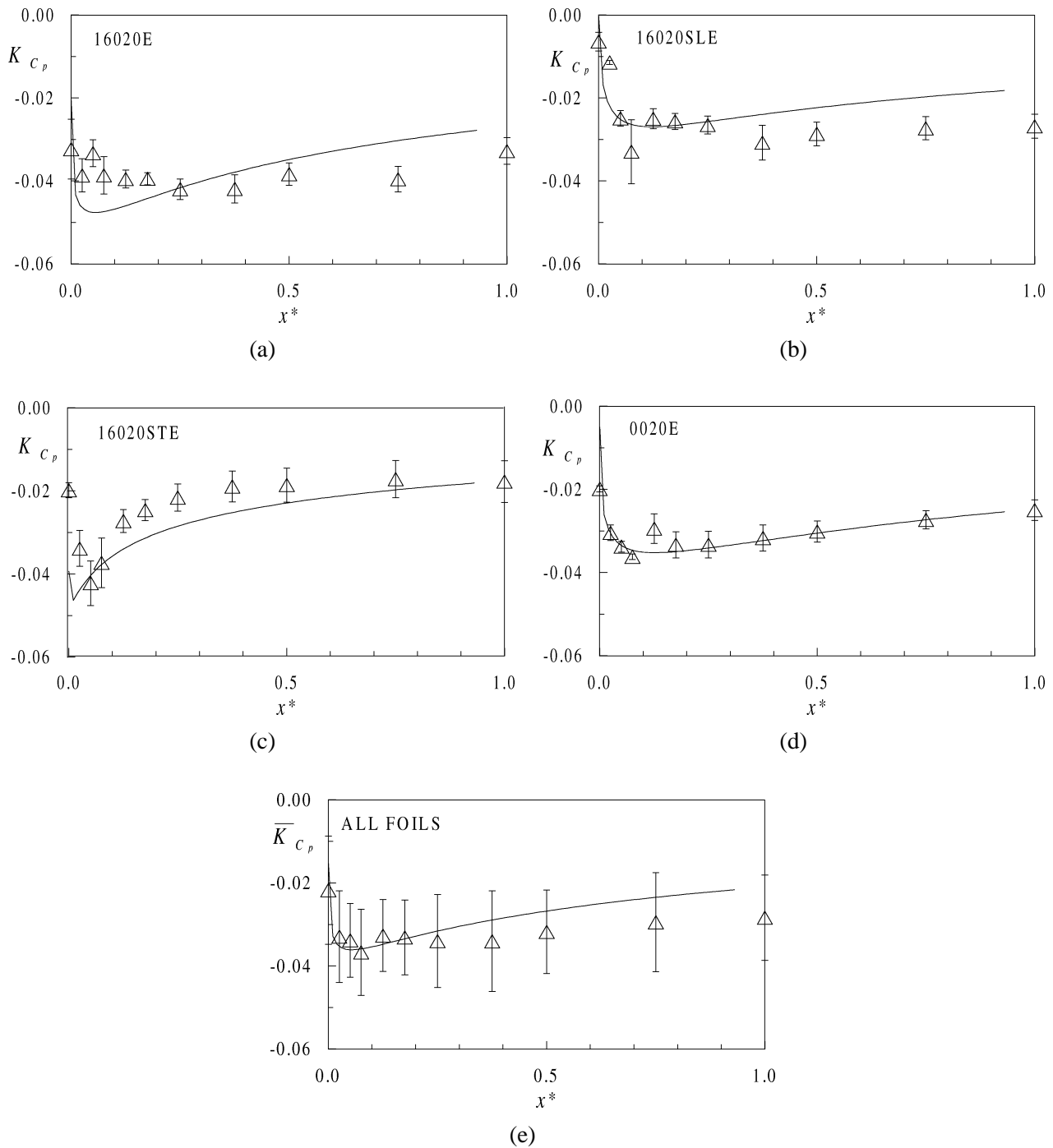
Figure 8. K_{C_P} as a function of the nondimensional distance from the foil. Continuous line is the model results. Symbols and vertical bars are the averaged experimental values and the standard deviations obtained from experimental conditions given on *table I*: (a) 16020E, (b) 16020SLE, (c) 16020STE, (d) 0020E, (e) mean values of K_{C_P} computed using the previous results for the model (continuous line) and the experimental data (symbols).

Table III. Model parameters, vortex core growth parameter, b_1^*, value of κ, nondimensional time of occurrence and location from the foil tip of the minimum pressure coefficient, value of $K_{C_{P_{\min}}}$ characteristic time of roll-up process and relative apparent viscosity computed for $Re = 10^6$.

Foil type	α_0	γ_0	α	γ	k_1	k_2	b_1^*	κ	$t_{\min}^*$	$x_{\min}^*$	$K_{C_{P_{\min}}}$	T^*	$\bar{\nu}_T/\nu$
16020E	0.36	0.18	1.61	2.00	0.25	7	0.784	0.670	0.041	0.06	−0.047	26.9	58.1
16020SLE	0.29	0.001[a]	3.31	550[a]	0.32	0.6	1.288	0.99	0.076	0.12	−0.027[b]	10.9	133.0
16020STE	0.40	0.28	1.07	0.53	−0.6	3	0.669	0.360	0.009	0.004	−0.046	554.1[a]	58.0
0020E	0.40	0.1	1.75	5.00	0.25	7	0.940	0.901	0.104	0.13	−0.035	10.5	70.2
16020POLY	0.50	0.18	1.78	2.88	−0.3	1	1.064	0.74	0.057	0.04	−0.033	6.3	102.4
Mean values	0.39	0.19	1.90	2.60	−0.02	3.72	0.95	0.73	0.06	0.07	−0.0376	13.65	84.4
Strd deviation	0.08	0.07	0.84	1.87	0.41	3.13	0.24	0.24	0.04	0.05	0.01	9.08	32.67

[a] Not used for mean values.

[b] In this case, since γ is out of the range for which Eq. (35) has been established, $K_{C_{P_{\min}}}$ was obtained by computing the minimum of the function in Eq. (12).

the same velocity data. As shown, the modeled pressure distributions along the vortex path are quite well representative of the experimental data. Comparing the various configurations studied, the pressure evolution differs depending on the foil planform and cross section. In particular the longitudinal pressure gradients at the tip and downstream the pressure minimum vary strongly. *Figure 8(e)* summarizes the results, showing the mean of K_{C_P} obtained from the previous curves, for both the model and the experimental data. As shown, the evolutions are in accordance. The experimental mean of $K_{C_{P_{\min}}}$ equal to −0.0376, is very close to that of the model equal to −0.0361 but off by about 18%, in absolute values, from the mean of K_{σ_d}, 0.043 (computed from data in *table I*). Interestingly enough, the values compare very favorably with $K_{\sigma_d} = 0.036$ obtained by Platzer and Souders [24] with a NACA66 (mod) elliptical foil at $Re = 5 \cdot 10^6$. Both values are still lower than the values of K_{σ_d} (equal to 0.073, 0.068 and 0.059) found by Maines and Arndt [10] (for 4215, 662-415 and 16-020 foils, respectively) at $Re = 0.48 \cdot 10^6$. However, in spite of the large range of experimental condition, the agreement between σ_d and $C_{P_{\min}}$ is satisfactory for results obtained in tests conducted at different laboratories, LEGI, ENSTA and GTH (see *figure 9* and *table IV*). The discrepancy, of about 18%, between $-C_{P_{\min}}$ and σ_d can be partly ascribed to the axisymmetric flow hypothesis. Relaxation of this hypothesis is one of the open possibilities to improve the methodology proposed here. Effect of spatial wandering or meandering on experimental laser velocimeter measurements which artificially enlarge the size of the measured vortices [4,29] and consequently influence the estimate of the pressure coefficient should be also examined.

The vortex growth parameter, b_1^*, ranges from 0.67, for the STE foil, to 1.3, for the SLE foil, with a mean value (see *table III*) close to one (0.949)). As shown in *figure 10(a)*, there is a clear trend indicating that the cavitation inception should be retarded when the values of b_1^* increase and as a result, foils developing tip vortices characterized by relatively large values of b_1 should be appropriate to delaying cavitation.

In figure 2 of Zeman [3] the values of b_1 obtained from Baker et al. [2], Baker et al.'s data correlate as $b_1 \sim 5(\Gamma_0/\nu)^{-0.5}$ for a foil operating at $Re = 10^4$. Using Eq. (17), with $b_1^* = 0.949$ and $Re = 10^4$, we find here $b_1 = 5.56 \, (\Gamma_0/\nu)^{-0.5}$. Taking into consideration that Zeman conditions are for the far field and ours conditions are for the near field, this result is rather encouraging and seems to indicate that the growth parameter seems to be quite universal and characterizes tip vortices in both the near and far field.

Finally, it is interesting to look on the effect of the apparent viscosity, $\bar{\nu}_T$, highly dependent on the foil planform, (see *table III*) since it ranges from 58ν, for the 16020E foil, to 133ν, for the 16020SLE foil, for $Re = 10^6$; thus, two orders of magnitude larger than the molecular viscosity. As shown in *figure 10(b)*, when $\bar{\nu}_T$
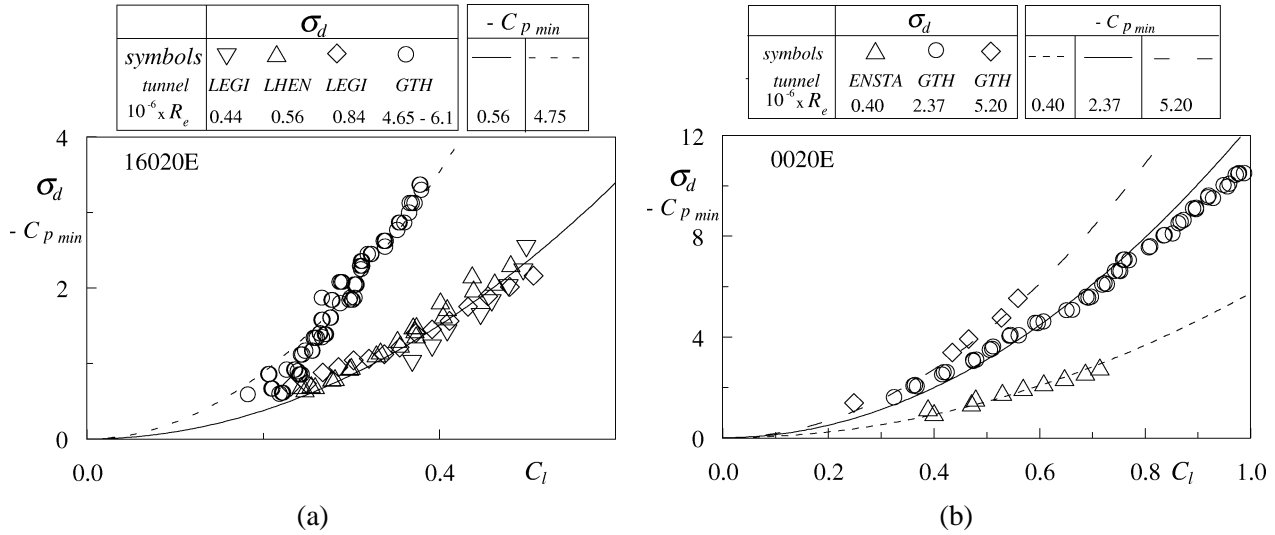
Figure 9. Experimental desinent cavitation number (symbols) and modeled minimum pressure coefficient (dashed and continuous lines) as a function of the lift coefficient (a) for the 16020E foil and (b) for the 0020E foil. Experimental data are adapted from the A.C.C. databank.
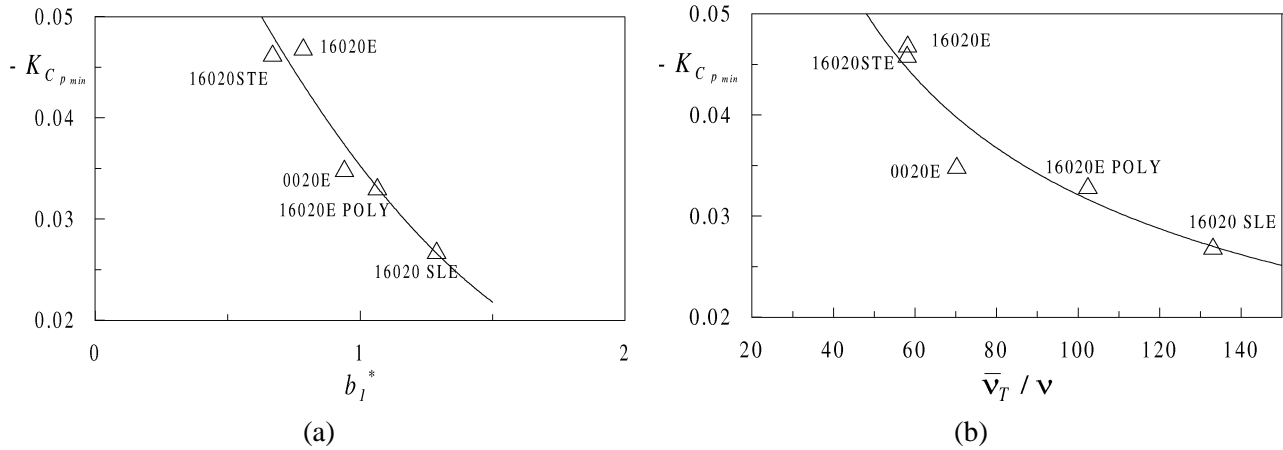

Figure 10. $K_{C_{P_{\min}}}$ as a function of: (a) the vortex growth rate; (b) the relative apparent viscosity.

Table IV. Values of K_{σ_d} obtained in different facilities at various Reynolds numbers for both cross sections. Mean value of K_{σ_d} and opposite of $K_{C_{P_{\min}}}$ obtained by the predictive model.

Foil	16020E				0020E		
Tunnel	LEGI		GTH		ENSTA	GTH	
$10^{-6} \times Re$	0.44	0.84	4.75	6.1	0.4	2.37	5.2
K_{σ_d}	0.0485	0.0399	0.0474	0.043	0.0338	0.0318	0.0364
mean value	0.0447				0.034		
$-K_{C_{P_{\min}}}$	0.0472				0.035		

increases, $K_{C_{P_{\min}}}$ decreases suggesting that an augmentation of the apparent viscosity may be a way to delay cavitation onset. According to Eq. (33), this is equivalent to an increase of α_0, α, or T^*.

6. Conclusions

Prediction of cavitation inception in wing tip vortices has been investigated. Using detailed tangential and axial velocity data in the very near region of tip vortices (for distances comprised between the foil tip and one maximum chord) issued from foils having an elliptical distribution of chord as well as two cross sections, and also using polymer solution ejection it has been possible to show that:

(a) The nondimensional radius of the tip vortex, a^* is a linear function of $(\Gamma^* t^*)^{0.5}$, where Γ^* is a nondimensional local vortex intensity and t^* the nondimensional time for a fluid particle to reach a given station along the vortex path.

(b) The zero ordinate is the initial core radius condition, and the slope is the vortex growth rate, b_1 which is found to be proportional to $(\Gamma_0/\nu)^{-0.5} Re^{0.3}$.

Based on the above findings, a model which enables the description of the evolution of the tip vortex characteristics and to estimate the value and the position of the minimum pressure coefficient along the vortex path has been developed. To achieve this, both the core radius and the vortex intensity are described by power law functions with the exponents selected in such a way that $a^* \sim (\Gamma^* t^*)^{0.5}$ is satisfied. For the considered experimental conditions, the model leads to the following conclusions:

(i) vortex diffusion, during the roll-up process, occurs as if the fluid had an apparent viscosity of about two orders of magnitude larger than the molecular viscosity,

(ii) the minimum pressure coefficient strongly depends on the initial conditions at the tip of the foil,

(iii) the modeled minimum pressure coefficient agrees well with the experimental desinent cavitation number obtained in various cavitation tunnels operating $4 \cdot 10^5 < Re < 6 \cdot 10^6$,

(iv) the minimum pressure occurs very close to the foil tip, within an interval ranging from one hundredth to one tenth of the maximum chord, and

(v) delaying cavitation inception can be achieved by increasing the vortex growth rate or the apparent viscosity.

It has to be stressed that, since the near field behavior of the tip vortices is very much dependent on the hydrofoil planform, cross section and tip geometry (for rectangular and trapezoidal foils in particular), the present results can only be employed for foils having an elliptical chord distribution. However, the approach to analyze the results is rather general and can be of great practical interest in most engineering situations. The authors pointed out that if the scaling relationships $(a \sim \delta, \ \Gamma \sim \Gamma_0)$ and the axisymmetric vortex flow $(C_P \sim (\Gamma/a)^2)$ can be hypothesized, the model can reasonably apply to other situations with different loading distributions.

Since only four parameters are needed (initial vortex parameters (α_0, γ_0) and vortex growth parameters (α, γ)) the model gives important trends which allow simple examination of conditions mitigating the occurrence of cavitation on lifting surfaces. Because it provides a concise presentation of the numerous cases investigated, the model can also be used as a guideline or as a benchmark by the developers of numerical codes which are capable of simulating tip vortex roll-up and diffusion in the near field.

Finally, the model could be improved to take into account of the existence, if any, of a non-axisymmetric vortex or a wandering effect in the region close to the wing tip which should affect the vortex core pressure estimate. More detailed experimental studies are required to deal with these issues.

Acknowledgements

References

[1] Chigier N.A, Corsiglia V.R., Wind-tunnel studies of wing wake turbulence, J. Aircraft 9 (12) (1972) 820–825.

[2] Baker G., Barker S.J., Bofah K.K., Saffman P.G., Laser anemometer measurements of trailing vortices in water, J. Fluid Mech. 65 (2) (1974) 325–336.

[3] Zeman O., The persistence of trailing vortices: A modeling study, Phys. Fluids 7 (1) (1995) 135–143.

[4] Devenport W.J., Rife M.C., Liapis S.I., Follin G.J., The structure and development of a wing-tip vortex, J. Fluid Mech. 312 (1996) 67–106.

[5] Billet M.L., Holl J.W., Scale effects on various types of limited cavitation, J. Fluid Eng-T ASME 103 (1981) 405–414.

[6] Stinebring D.R., Farell K.J., Billet M.L., The structure of a three dimensional tip vortex at high-Reynolds number, J. Fluid Eng-T ASME 113 (1991) 496–503.

[7] Fruman D.H., Dugué C., Pauchet A., Cerrutti P., Briançon-Marjollet L., Tip vortex roll-up and cavitation, in: 19th Symposium on Naval Hydrodynamics, Seoul, 1992.

[8] Maines B.H., Arndt R.E.A., Bubble dynamics of cavitation inception in a wing tip vortex, ASME FED 153 (1993) 93–97.

[9] Maines B.H., Arndt R.E.A., Viscous effects on tip vortex cavitation, ASME FED 177 (1993) 125–132.

[10] Maines B.H., Arndt R.E.A., Tip vortex formation and cavitation, J. Fluid Eng-T ASME 119 (1997) 413–419.

[11] A.C.C. databank, http://www.ecole-navale.fr/bank.acc.htlm (on request).

[12] Fruman D.H., The "Action Concertée Cavitation" research program and accomplishments, in: Proceedings of 5th International Symposium on Cavitation, CAV'95, Deauville, France, 1995, pp. 211–217.

[13] Fruman D.H., Cerrutti P., Pichon T., Dupont P., Effect of hydrofoil planform on tip vortex roll-up and cavitation, J. Fluid Eng-T ASME 117 (1) (1995) 162–169.

[14] Pauchet A., Briançon-Marjollet L., Gowing S., Cerrutti P., Pichon T., Effect of foil size and shape on tip vortex cavitation occurrence, in: Proceedings of 2nd International Symposium on Cavitation, Tokyo, Japan, 1994.

[15] Pichon T., Pauchet A., Astolfi J.-A., Fruman D.H., Billard J.-Y., Effect of tripping laminar-to-turbulent boundary layer transition on tip vortex cavitation, J. Ship Res. 41 (1) (1997) 1–9.

[16] Pauchet A., Viot X., Fruman D.H., Effect of upstream turbulence on tip vortex roll-up and cavitation, in: ASME Cavitation and Multiphase Flow Forum, San Diego, CA, USA, 1996.

[17] Boulon O., Franc J.-P., Lami P., Michel J.-M., Mory M., Tip vortex cavitation on an oscillating hydrofoil, in: Proceedings of 5th International Symposium on Cavitation, CAV'95, Deauville, France, 1995, pp. 145–152.

[18] Boulon O., Franc J.-P., Michel J.-M., Effet du confinement sur la cavitation de tourbillon marginal, in: 3èmes journées cavitation, Colloque de la Société Hydrotechnique de France, Grenoble, Publications S.H.F, 1996, pp. 51–60.

[19] Deniset F., Pellone C., Confinement influence on tip vortex development, in: Proceedings of 5th International Symposium on Cavitation, CAV'95, Deauville, France, 1995, pp. 425–432.

[20] Gowing S., Briançon-Marjollet L., Frechou D., Godefrroy V., Dissolved gas and nuclei effects on tip vortex cavitation inception and cavitating core size, in: Proceedings of 5th International Symposium on Cavitation, CAV'95, Deauville, France, 1995, pp. 173–180.

[21] Briancon-Marjollet L., Merle L., Inception, development, and noise of a tip vortex cavitation, in: 20th Symposium on Naval Hydrodynamics, Trondheim, Norway, 1996, pp. 278–290.

[22] Fruman D.H., Pichon T., Cerrutti P., Effect of a drag-reducing polymer solution on tip vortex cavitation, J. Mar. Sci. Technol. 1 (1995) 13–23.

[23] McCormick B.W., On cavitation produced by a vortex trailing from a lifting surface, J. Basic Eng. (September 1962) 369–379.

[24] Platzer G.P., Souders, W.G., Tip vortex cavitation characteristics and delay on a three-dimensional hydrofoil, in: 19th American Towing Tank Conference, 1980.

[25] Arakeri V.H., Higuchi H., Arndt R.E.A., A model for predicting tip vortex cavitation characteristics, J. Fluid Eng-T ASME 110 (1988) 190–193.

[26] Hsu C.C., Studies of scaling of tip vortex cavitation inception on marine lifting surfaces, J. Fluid Eng-T ASME 113 (1991) 504–508.

[27] Ferreira De Sousa P.J.S.A., Falcao De Campos J.A.C., A method for the prediction of the minimum pressure in tip vortices from three-dimensional foils, in: ASME 1996, FED-Vol. 236, Fluids Engineering Division Conference, 1, 1996, pp. 471–478.

[28] Viot X., Jeanson C., Fruman D.H., Investigation of tip vortex cavitation by hydrofoil fractionation, in: ASME FED, Vancouver, Canada, June 1997, pp. 22–26.

[29] Straka W.A., Farrell K.J., The effect of spatial wandering on experimental laser velocimeter measurements of the end-wall vortices in an axial-flow pump, Exper. Fluids 13 (1992) 163–170.